ELSEVIER

Physica B 297 (2001) 226–233

PHYSICA B

www.elsevier.com/locate/physb

Small-angle neutron scattering investigations of magnetic nanostructures and interfaces using polarized neutrons

Albrecht Wiedenmann*

Hahn-Meitner-Institut Berlin, Glienickerstrasse 100, D-14109 Berlin, Germany

Abstract

Using polarized neutrons, the relative contrasts for small-angle scattering are strongly modified which allows a precise evaluation of magnetization, density and composition profiles at surfaces and interfaces of nanoscaled materials. In Co ferrofluids, the magnetic core behaves as a non-interacting single domain. The core is encapsulated by a shell of surfactant molecules which was found to be impenetrable for the solvent. In soft magnetic Fe–Si–B–(Nb,Cu) and Fe–Nb–B alloys, the presence of a weak magnetic interface between ferromagnetic nanocrystals and amorphous matrix has been demonstrated which breaks the exchange interactions.

Keywords: Magnetic nanostructures; Polarized neutrons; Small-angle neutron scattering

1. Introduction

Small-angle neutron scattering (SANS) studies are presented on nanoscaled (n-) materials with single-domain magnetic particles where we face the problem that weak magnetic scattering signals have to be analyzed besides strong contributions from other sources or vice versa. We demonstrate that polarized neutrons modify the relative scattering contrasts, providing information unavailable in conventional SANS.

2. Small-angle neutron scattering cross-sections

Elastic scattering of neutrons with wavelength λ at an angle 2θ leads to the momentum transfer of magnitude $Q = 4\pi \sin(\theta)/\lambda$ and hence, to the phase shift of $\exp(i\boldsymbol{Qr})$. The SANS cross section is obtained by summing up the scattering amplitudes of all atoms weighted by the phase shift at each atomic position $\boldsymbol{r}$. The form factors for nuclear (F_N) and magnetic (F_M) scattering for a particle of species j embedded in a homogeneous matrix are given by

$$F_j = \int_{pj} \mathrm{d}\boldsymbol{r}\eta_j \exp(i\boldsymbol{Q}\cdot\boldsymbol{r}_j) = \Delta\eta_j V_{pj} f(QR),$$

where V_{pj} is the volume of the particle and $f(QR)$ depends only on its shape. The contrast $\Delta\eta$ is the difference between the scattering length densities of particle and matrix, $\Delta\eta = \eta_p - \eta_{\mathrm{matrix}}$. For nuclear scattering $\eta_N = \sum c_i b_i/\Omega_i$ where b_i is the nuclear scattering length, c_i the atomic concentration and Ω_i the atomic volume of constituent i. Similarly, a magnetic scattering amplitude is defined by $\eta_M = (0.27 \times 10^{-12}\ \mathrm{cm})\sum c_i \boldsymbol{M}_i^{\perp}/\Omega_i$, where $\boldsymbol{M}_i^{\perp}$ (in Bohr magnetons) is the projection of the

* Fax: +49-30-80-62-3059.
E-mail address: Wiedenmann@hmi.de (A. Wiedenmann).

0921-4526/01/$ - see front matter
PII: S0921-4526(00)00872-3

moment on a plane perpendicular to the scattering vector $\boldsymbol{Q}$.

For polarized neutrons where the neutron spins are aligned antiparallel (denoted by $+$) or parallel ($-$) to a preferred orientation $z\|\boldsymbol{H}$ (where $\boldsymbol{H}$ is the magnetic field vector), four types of scattering processes have to be distinguished, two for conserving the neutron spin (spin non-flip scattering: snf) and two with reversal of the spin by the scattering (spin-flip scattering: sf) [1,2]. When the polarization of the *scattered* neutrons is not analyzed (denoted here as SANSPOL), the intensity collected in the detector contains snf and sf contributions and depends on the polarization state of the incident neutrons, i.e. $I^{+}(Q,\alpha) = \langle|F^{++}|^2\rangle + \langle|F^{+-}|^2\rangle$ and $I^{-}(Q,\alpha) = \langle|F^{--}|^2\rangle + \langle|F^{-+}|^2\rangle$, respectively. These averages have been given in Ref. [3] for the case where the magnetic moments and neutron polarization are fully aligned along the external field. We consider here the case of *non-perfect alignment* of the magnetic moments of a non-interacting ferromagnetic single-domain particles of saturation magnetization M_s^p embedded in a matrix of magnetization $M_s^m = cM_s^p$. For such superparamagnetic particles, the orientation distribution of the magnetic moments as a function of an effective magnetic field H_{eff} and temperature follows the Langevin statistics $L(x) = \coth(x) - 1/x$, with the argument $x = M(R')H_{\mathrm{eff}}/k_B T$. The total moment, $M(R')$, depends on the radius R' of the particles according to $M(R') = 4\pi R'^3 m_0/3\Omega_{\mathrm{at.}}$, where m_0 is the saturation value of the atomic magnetic moment. Neglecting second-order interference effects between scattered and non-scattered neutrons [4] and using the formalism presented in Ref. [5] SANSPOL cross-sections for the case of a dilute system of non-interacting particles are given by

$$\begin{aligned} I^{+}(Q,\alpha) &= F_N^2 + F_M^2 2L(x)/x \\ &\quad + \left\{F_M^2\left(c^2 - 2L(x)c + 1 - \frac{3L(x)}{x}\right)\right. \\ &\quad \left. - 2PF_N F_M(L(x) - c)\right\}\sin^2\alpha, \\ I^{-}(Q,\alpha) &= F_N^2 + F_M^2 2L(x)/x \\ &\quad + \left\{F_M^2\left(c^2 - 2L(x)c + 1 - \frac{3L(x)}{x}\right)\right. \\ &\quad \left. + 2P\varepsilon F_N F_M(L(x) - c)\right\}\sin^2\alpha. \end{aligned} \tag{1a}$$

α is the azimuth angle between $\boldsymbol{H}$ and $\boldsymbol{Q}$ and P is the polarization defined by $P = (n^{+} - n^{-})/(n^{+} + n^{-})$ where n^{+} is the number of neutrons with spin antiparallel, and n^{-} the number of neutrons with spin parallel to $\boldsymbol{H}$. The reversal of the polarization direction is achieved with a spin-flipper of efficiency ε. The arithmetic mean of the intensities $[I^{+}(Q,\alpha) + I^{-}(Q,\alpha)]/2$ corresponds to the intensity of a non-polarized beam,

$$\begin{aligned} [I^{+}(Q,\alpha) + I^{-}(Q,\alpha)]/2 &= I(Q,\alpha)_{\text{non-polarized}} \\ &= A(Q) + B(Q)\sin^2\alpha. \end{aligned} \tag{1b}$$

The difference between the intensities of the two polarization states represents a magnetic–nuclear cross term,

$$\begin{aligned} I^{-}(Q,\alpha) - I^{+}(Q,\alpha) &= 2P(1+\varepsilon)F_N F_M[L(x) - c] \\ &\quad \times \sin^2\alpha = B_{\mathrm{int}}(Q)\sin^2\alpha. \end{aligned} \tag{1c}$$

Owing to the vector nature of $\boldsymbol{F}_M^{\perp}(Q)$, the scattering profiles [Eqs. (1a)–(1c)] are anisotropic and described by

$$\mathrm{d}\sigma/\mathrm{d}\Omega(Q) = A(Q) + B^{\pm}(Q)\sin^2\alpha. \tag{2}$$

The isotropic term $A(Q) = F_N^2 + F_M^2 2L(x)/x$ is independent of the polarization state and beside the nuclear term F_N^2 contains an additional term of magnetic origin (which vanishes for $L(x)/x = 0$ i.e. for complete alignment of all moments along $\boldsymbol{H}$). The anisotropic part $B^{\pm}(Q)$ is different for the two polarization states. The cross-term $B_{\mathrm{int}}(Q)$ in Eq. (1c) is linear in the magnetic amplitude. Thus, with polarized neutrons it is possible to determine the absolute value of the magnetic contrast with respect to the nuclear contrast, i.e. magnetization and compositions of particles and matrix. The ratio $\gamma = F_M/F_N$ between the magnetic and nuclear form factors is directly related to the intensity ratio of both polarization directions ("flipping- ratio" FR) for $\boldsymbol{Q}$ perpendicular to $\boldsymbol{H}$ ($\alpha = \pi/2$),

$$\begin{aligned} FR &= \frac{I^{-}(\boldsymbol{Q}\perp\boldsymbol{H})}{I^{+}(\boldsymbol{Q}\perp\boldsymbol{H})} \\ &= \frac{1 + 2P\varepsilon\gamma(L(x) - c) + e(x)\gamma^2}{1 - 2P\gamma(L(x) - c) + e(x)\gamma^2}, \end{aligned} \tag{3}$$

where $e = [1 + c^2 - 2L(x)c - L(x)/x]$. The quantities $I^{\pm}(Q)$ can be measured very precisely from

the analysis of the whole 2D pattern according to Eq. (2). Consequently, the magnitude of γ can be determined much more accurately by SANSPOL than for non-polarized neutrons, for which $|\gamma| = [B(Q)/A(Q)]^{1/2}$.

3. Experimental

SANS measurements have been performed at the instrument V4 installed at the BERII reactor of HMI, Berlin. A horizontal magnetic field of strength up to 1.1 T was applied at the sample position, oriented perpendicular to the incoming neutrons. Polarized neutrons (n^+) are provided by a transmission polarizing super-mirror cavity. The polarization direction is reversed using a spin flipper in front of the sample. The SANSPOL option, which can be set without any modification of the instrument alignment, is characterized by a high-neutron flux of more than 30% of non-polarized neutrons, a high degree of polarization ($P > 90\%$) at all accessible wavelengths and by the high efficiency of the spin flipper ($\varepsilon > 95\%$) [6]. The reliability of this option has been demonstrated recently by comparing the results of a SANSPOL study on magnetic glass ceramics to those of a conventional SANS study [3].

4. Cobalt ferrofluids

"Ferrofluids" are colloidal magnetic solution where ferromagnetic nanosized particles are surrounded by organic chain molecules which act as surfactant and prevent the coagulation. We performed a SANS study on dilute solutions (1 vol%) of Co–(C_{21}–H_{39}–N–O_3) in four different mixtures of protonated and deuterated toluene, denoted as AF1–AF4 (Table 1). In a first conventional SANS study of the sample AF4 nuclear and magnetic scattering contributions have been extracted and analyzed in terms of number-distributions $N(R)$ of non-interacting spherical particles. For the magnetic contribution a maximum of $N_{\mathrm{mag}}(R)$ appeared at $R = 3.3$ nm whereas from the nuclear contribution, which is dominated by the high level of the incoherent background (mainly from hydrogen contained in the solvent and surfactant) a bimodal distribution had to be assumed with maxima at $R_1 = 1.12$ nm and $R_2 = 4.9$ nm.

The two-dimensional SANSPOL pattern for AF4 shown in Fig. 1 are highly anisotropic with a dramatic change of the aspect ratios for the two polarization states. We emphasize the particularity that only for the polarization state I^- a maximum appears in the outer part of the patterns. The difference signal ($I^- - I^+$) of Fig. 1 shows the $\sin^2\alpha$ behavior expected from Eq. (1c) with negligible intensity along the direction of the magnetic field. Note the negative values in the inner part and positive values in the outer part. The SANSPOL intensities perpendicular to the applied field $I^{\pm}(\boldsymbol{Q}\perp\boldsymbol{H})$ as obtained by an adjustment of the 2-d pattern to the angular dependence given in Eq. (2) are compared for the different solvents in Fig. 2a. In the fully (AF2) and partly deuterated solvents (AF4, AF3) pronounced maxima occur only for $I^-(\boldsymbol{Q}\perp\boldsymbol{H})$ whereas $I^+(\boldsymbol{Q}\perp\boldsymbol{H})$ decreases always continuously with increasing Q. The position of the maximum of $I^-(\boldsymbol{Q}\perp\boldsymbol{H})$ shifts to lower Q for increasing content of hydrogen. The cross-term B_{int} reverses

Table 1
Scattering length densities as obtained from a fit to a shell model using the bulk value of η_1 (nuclear) $= 2.53 \times 10^{10}$ cm^{-2} for Co

Sample	Content C_7D_8 (%)	η (solvent) 10^{10} cm^{-2}	η_1 (mag) 10^{10} cm^{-2} SANSPOL	η (mag) 10^{10} cm^{-2} SANS	η_2 (shell) 10^{10} cm^{-2}
AF2	100	5.65	4.29	4.38	0.56
AF4	43	3.0	4.5	5.3	0.3
AF3	14	1.6	1.52	1.62	0.9
AF1	0	0.97	0.94	1.24	0.8

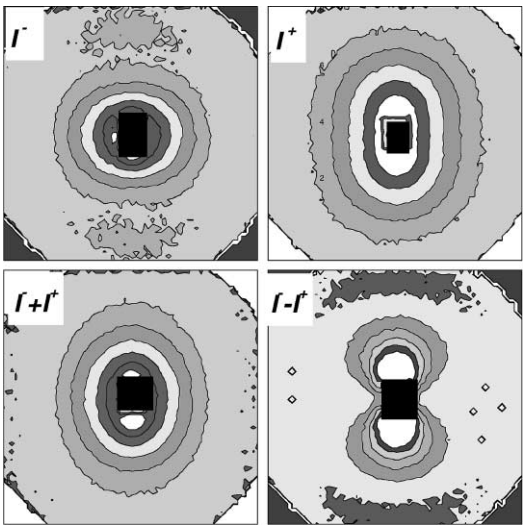

Fig. 1. SANSPOL patterns in Co ferrofluid AF4 for neutron spins antiparallel (I^-) and parallel (I^+) to the horizontal field of strength $H = 1.1$ T. The arithmetic mean $[(I^-) + (I^+)]/2$ corresponds to the 2D pattern of non-polarized neutrons. The difference $(I^-) - (I^+)$ yields the interference term [Eq. (1c)] with negative values in the center (green–blue).

the sign from negative values below $Q = 0.61\ \mathrm{nm}^{-1}$ to positive values above, with a maximum at $Q = 0.8\ \mathrm{nm}^{-1}$ (Fig. 3). For Q larger than $1.35\ \mathrm{nm}^{-1}$, B_{int} is zero, which proves that there is no magnetic contribution left. The ferrofluid AF1 in a fully protonated solvent shows only a splitting of $I^+(\boldsymbol{Q}\perp\boldsymbol{H})$ and $I^-(\boldsymbol{Q}\perp\boldsymbol{H})$ below $Q = 1\ \mathrm{nm}^{-1}$, where $I^-(\boldsymbol{Q}\perp\boldsymbol{H}) > I^+(\boldsymbol{Q}\perp\boldsymbol{H})$. The flipping ratio FR derived from Eq. 3 (Fig. 2b) are different for each solvent at low Q but follow nearly the same Q dependence at high Q. This indicates that the surface of the magnetic Co particles must be surrounded by a layer of almost constant density different from that of the solvent.

While from non-polarized neutrons size distributions corresponding to individual nuclear and magnetic units are derived, polarized neutrons show that both contributions must result from a "composite" particle built up by a magnetized core of Co atoms surrounded by a nonmagnetic surface layer. As the simplest description for such a "composite" we use a shell model consisting of a sphere with an inner core radius R' surrounded by a concentric shell of radius R. The form factor is

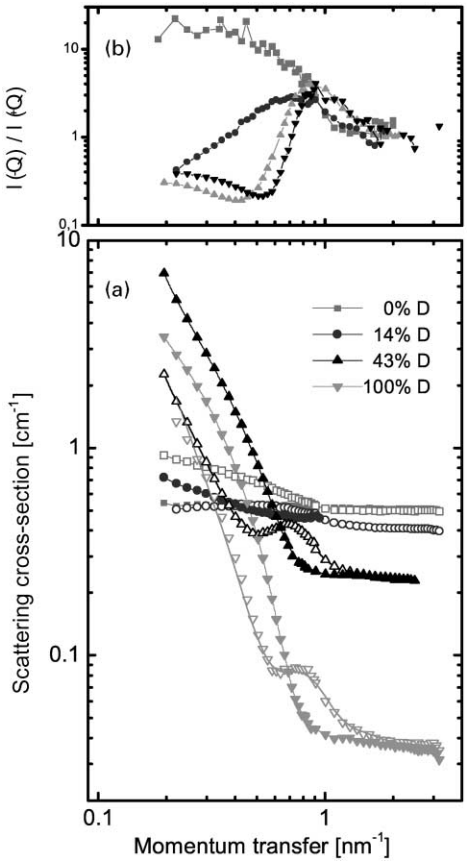

Fig. 2. SANSPOL of Co ferrofluids in different mixtures of C_7D_8–C_7H_8. (a) Intensities $I^+(\boldsymbol{Q}\perp\boldsymbol{H})$ (solid symbols) and $I^-(\boldsymbol{Q}\perp\boldsymbol{H})$ (open symbols). Solid lines: Fit according to a shell model using the parameters Table 1. (b) Flipping ratio.

given by

$$F_{\mathrm{shell}}(Q) = [(\Delta\eta_1 - \Delta\eta_2) f_{\mathrm{sph}}(QR') + \Delta\eta_2 f_{\mathrm{sph}}(QR)] V_p$$

with

$$f_{\mathrm{sph}}(x) = 3[\sin(x) - x\cos(x)]\ x^{-3}. \quad (4)$$

The scattering contrasts with respect to the matrix are different for the magnetic core and non-magnetic shell and given by $\Delta\eta_1^{(\pm)} = \eta_1^{\mathrm{nuc}} \pm \eta_1^{\mathrm{mag}} - \eta_{\mathrm{matrix}}$ and $\Delta\eta_2 = \eta_2^{\mathrm{nuc}} - \eta_{\mathrm{matrix}}$, respectively. In the present case, only $\Delta\eta_1^{(\pm)}$ depends on the polarization. The intensities were calculated according to $I(\boldsymbol{Q}\perp\boldsymbol{H}) = N_{\mathrm{p}} \int F_{\mathrm{shell}}^2(Q, R) N(R')\, \mathrm{d}R$, ($N_{\mathrm{p}}$ is the number density of particles in the beam), assuming

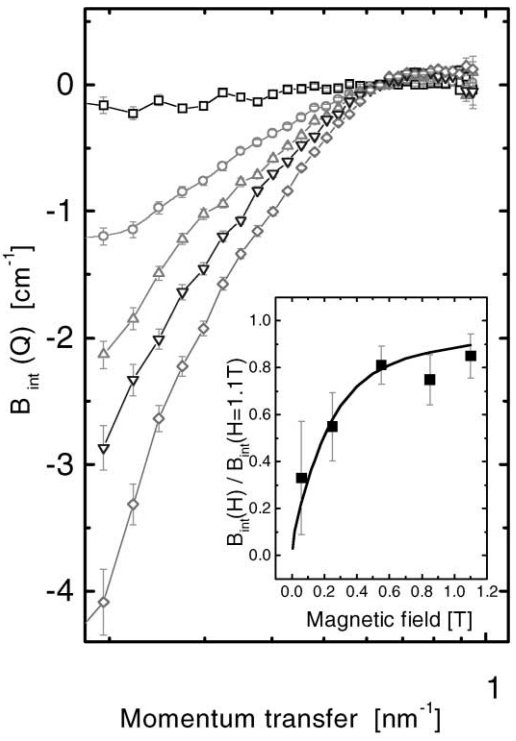

Fig. 3. Cross-term $B_{\rm int}(Q)$ for Co ferrofluid AF4 as a function of Q at $H = 1.1$ T ($\diamond$), 0.85 T ($\triangledown$), 0.25 T ($\triangle$), 0.06 T ($\bigcirc$) and 0 T ($\square$). Insert: Field variation of the ratio $B_{\rm int}(Q,H))/B_{\rm int}$ $(Q, H = 1.1$ T) (symbols) follows the Langevin behavior for non-interacting single-domains particles of $\langle R\rangle = 3.7$ nm (solid line).

a log-normal number distribution of the core radius $N(R')$ and a constant thickness of the shell, i.e. $R = R' + dR$. The parameters $N_{\rm p}$, R', dR and the width of the size distribution s were constrained to be identical for both polarization states and the contrasts $\Delta\eta_1^{(\pm)}$ and $\Delta\eta_2$ have been adjusted in a non-linear least-squares fitting routine. The solid lines in Fig. 2 represent the calculated intensities $I^{\pm}(\boldsymbol{Q}\perp\boldsymbol{H})$. It turned out that for all solvents this simple model function lead to consistent parameters, i.e. a rather sharp distribution $N(R')$ corresponding to a volume weighted average of the core radius of $\langle R'\rangle = 3.7$ nm and a constant thickness of the shell of d$R = 2.47$ nm. We emphasize that from non-polarized neutrons alone it would not have been possible to derive the shell model due to the very low nuclear contrast beside the high incoherent background. The first maximum of the size distribution of spheres as obtained from classical SANS must therefore be artificial and reflects in fact half of the thickness of the shell.

The scattering length densities resulting from fits of both polarization states using the same model function are included in Table 1. The values of η_2 for the shell of the same order of magnitude as calculated for densely packed surfactant molecules ($\eta_2 = 0.33 \times 10^{10}$ cm^{-2}) and do not depend significantly on the solvent composition. This supports strongly the conclusion that the organic surfactant is nearly impenetrable for the solvent in a shell of thickness of about 2.4 nm i.e. that the Co-core is not in direct contact with the solvent. The values of η_1(mag) in AF2 and AF4 experimentally derived at $H = 1.1$ T correspond closely to $\eta_1(\text{mag}) = 4.14 \times 10^{10}$ cm^{-2} expected for bulk Co ($m_0 = 1.715\,\mu_{\rm B}$/atom, $\Omega_{\rm at}$ (Co) $= 0.01099$ nm^3/at.) Discrepancies appeared in the samples AF1 and AF3 where much lower values for η_1(mag) were found. The reason for such anomalous low values is not yet clear; it might result from a lower particle density, to some oxidation, or to non-magnetic amorphous surface layers as reported for magnetic glass ceramics [7]. For the solvent composition AF4 the cross-term $B_{\rm int}(Q,H)$ has been evaluated for different values of the external magnetic field and plotted in Fig. 3. The ratio $B_{\rm int}(Q,H)/B_{\rm int}(Q,H = 1.1T)$ was found to be constant for all values of Q, the H-dependence of which follow roughly a Langevin function calculated assuming spherical Co particles with $\langle R\rangle = 3.7$ nm (inset Fig. 3). This is in good agreement with the prediction of Eq. (1c) (for the diamagnetic matrix $c = M_{\rm s}^{\rm m}/M_{\rm s}^{\rm p} = 0$) and with $\langle R'\rangle$ obtained from the model fit.

5. Weak magnetic interfaces in soft magnetic metallic glasses

Nanocrystalline Fe–Si–B-based alloys with small additions of Cu, Nb or W and Fe–M–B alloys (M:Zr,Nd,Hf) produced by controlled annealing of melt-spun amorphous alloys are well-known for their excellent soft magnetic properties. A conventional SANS study [8] on $Fe_{0.834}Si_{0.155}B_{0.07}Nb_{0.03}Cu_{0.01}$ revealed the

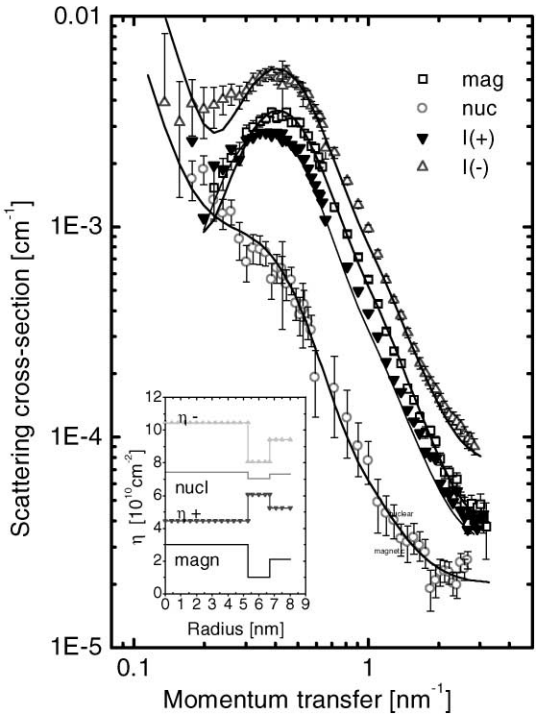

Fig. 4. Intensities $I^{-}(\boldsymbol{Q}\perp\boldsymbol{H})$, $I^{+}(\boldsymbol{Q}\perp\boldsymbol{H})$, I_{nuc} and I_{mag} for Fe–Si–B–Nb–Cu. Solid lines: fit with shell model using the parameters shown in the inset.

presence of a high volume fraction of ultra-fine grained Fe_3Si particles embedded in an amorphous matrix and suggested the presence of a weakly magnetic or paramagnetic interface [5]. SANSPOL allows us to study the presumed interface using a sample with a very low fraction of Fe_3Si nanocrystals of about 1 vol%. The intensities $I^{-,+}(\boldsymbol{Q}\perp\boldsymbol{H})$ are plotted in Fig. 4. For both polarization states a pronounced maximum occurs around $Q = 0.4\ \mathrm{nm}^{-1}$, i.e. at the same position at which a shoulder is found in the nuclear contribution $A(Q)$, as obtained separately from the sum signal (Eq. (1b)). The cross-term $B_{\mathrm{int}}(Q) > 0$, i.e. the sign of γ must be positive. In the diluted alloy where inter-particle interference effects can certainly be neglected the observed maxima must be related to the particle form-factor itself. We use again the simple shell model [Eq. (5)] where both the contrast $\eta_1^{(\pm)} = \eta_1^{\mathrm{nuc}} \pm \eta_1^{\mathrm{mag}} - \eta_{\mathrm{matrix}}$ for the core and $\Delta\eta_2^{(\pm)} = \eta_2^{\mathrm{nuc}} \pm \eta_2^{\mathrm{mag}} - \eta_{\mathrm{matrix}}$ for the shell depend on the polarization state since the matrix is ferromagnetic, i.e. $\eta_{\mathrm{matrix}}^{(\pm)} = \eta_{\mathrm{matrix}}^{\mathrm{nuc}} \pm \eta_{\mathrm{matrix}}^{\mathrm{mag}}$. The intensities were calculated assuming $R' = nR$ (solid lines in Fig. 4) leading to the contrasts $\Delta\eta_1^{(\pm)}$ and $\Delta\eta_2^{(\pm)}$ reported in Table 2. Nuclear and magnetic contrast are derived according to $\Delta\eta_i^{\mathrm{nuc}} = 0.5(\Delta\eta_i^{(+)} + \Delta\eta_i^{(-)})$ and $\Delta\eta_i^{\mathrm{mag}} = 0.5(\Delta\eta_i^{(-)} - \Delta\eta_i^{(+)})$, respectively, with much higher precision than from non-polarized SANS using the same model function. (see Table 2). The ratio between the magnetic contrasts of core and shell is given by $\Delta\eta_1^{\mathrm{mag}}/\Delta\eta_2^{\mathrm{mag}} = (1-c)/(c-d)$ and depends only on the ratio $c = \eta_{\mathrm{matrix}}^{\mathrm{mag}}/\eta_1^{\mathrm{mag}}$ and $d = \eta_2^{\mathrm{mag}}/\eta_1^{\mathrm{mag}}$. Using $c = 0.7$ as obtained from saturation magnetization of Fe_3Si and of the amorphous alloy of matrix composition we derive a very low value of $d = 0.35$. Using the theoretical values of $\eta_1^{\mathrm{nuc}} = 7.45 \times 10^{10}\ \mathrm{cm}^{-2}$ and $\eta_1^{\mathrm{mag}} = 3 \times 10^{10}\ \mathrm{cm}^{-2}$ the scattering length densities are obtained in absolute units from Table 2 and presented in the inset of Fig. 4, which shows the depletion of η_2. Using a more realistic density profile corresponding to a diffusion zone gives very similar results [9].

A comprehensive study of the evolution of the microstructure during annealing is currently undertaken in the soft magnetic alloy $Fe_{0.805}Nb_{0.07}B_{0.125}$ prepared by planar flow casting [10]. As an example, we present in Fig. 5 the SANS result obtained after annealing at 510°C for 1 h. Here again, the nuclear scattering contribution is nearly by one order of magnitude lower than the magnetic contribution. The SANSPOL intensities are very close to each other but $I^{-}(\boldsymbol{Q}\perp\boldsymbol{H})$ is always higher than $I^{\pm}(\boldsymbol{Q}\perp\boldsymbol{H})$. Correspondingly, the cross-term $B_{\mathrm{int}}(Q)$ is very weak but clearly it presents a maximum at $Q = 0.4\ \mathrm{nm}^{-1}$ in contrast to the curve calculated according to $2P(1+\varepsilon)(I_{\mathrm{nuc}}(Q)I_{\mathrm{mag}}(Q))^{0.5}$ from SANS results. Fitted parameters using the shell model are reported in Table 2. The nuclear contrast from nanocrystalline BCC-Fe embedded in the amorphous matrix turned out to be extremely low. Note the much higher values of $\Delta\eta_1^{\mathrm{nuc}}$ from SANS with respect to that of the SANSPOL analysis. This discrepancy indicates the presence of some non-magnetic impurity phase like oxides. The nuclear form-factor of such particles does not interfere with the magnetic form-factor of the Fe crystallites and hence would not contribute to $B_{\mathrm{int}}(Q)$. From the

Table 2
Contrasts [a.u.] from SANSPOL and SANS adjustments using log-normal distributions corresponding to average radii $\langle R\rangle = [\int N(R)R^3\ \mathrm{d}R/\int N(R)\ \mathrm{d}R]^{1/3}$

	$\langle R\rangle$ (nm)	$\Delta\eta_i^{(-)}$	$\Delta\eta_i^{(+)}$	$\Delta\eta_i^{\mathrm{nuc}}$ SANSPOL	$\Delta\eta_i^{\mathrm{mag}}$ SANSPOL	$\Delta\eta_i^{\mathrm{nuc}}$ SANS	$\Delta\eta_i^{\mathrm{mag}}$ SANS
Fe–Si–B							
Core	5.37	− 3.42	2.59	− 0.42	− 3.0	− 1.1	− 2.8
Shell	6.9	4.32	− 2.47	0.93	3.39	0.98	3.5
Fe–Nb–B							
Core	3.84	4.04	− 3.93	0.03	3.98	1.31	3.77
Shell	6.13	− 1.40	1.23	− 0.08	− 1.31	− 0.04	− 1.36

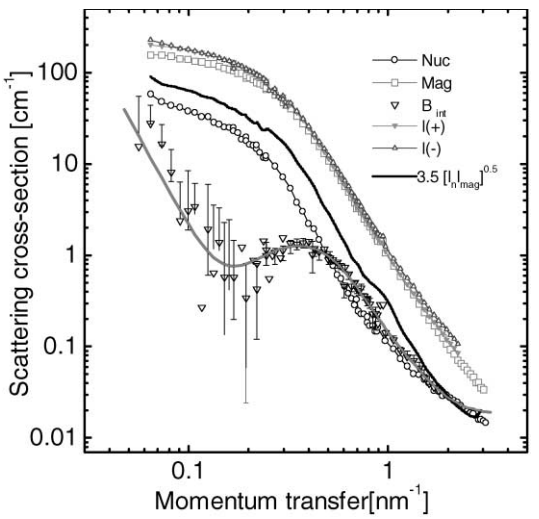

Fig. 5. SANSPOL intensities $I^-(\boldsymbol{Q}\perp\boldsymbol{H})$, $I^+,(\boldsymbol{Q}\perp\boldsymbol{H})$ and $B_{\mathrm{int}}(Q)$ compared to SANS results I_{nuc}, I_{mag} for soft magnetic Fe–Nb–B. The deviation of the cross-term $B_{\mathrm{int}}(Q)$ from $3.5(I_{\mathrm{nuc}}I_{\mathrm{mag}})^{0.5}$ (solid line) indicates the presence of an additional non-magnetic phase.

ratio $\Delta\eta_1^{\mathrm{mag}}/\Delta\eta_2^{\mathrm{mag}} = 2.9$, we derive again a low value of $d = 0.6$ assuming $c = 0.7$ as in the cases of Fe–Si–B–Cu–Nb alloy.

6. Summary

In SANSPOL the relative contrasts are strongly modified which allows any chemical or magnetization gradients to be established more precisely than in conventional SANS. The examples presented show that a simple shell model reproduces the basic features of such profiles. Co ferrofluids consist of "composite particles" formed by a magneticorę of average radius of $\langle R'\rangle = 3.7$ nm and surrounded by a shell of organic surfactant which, within a thickness of 2.4 nm is nearly impenetrable for the solvent. Superparamagnetic behavior of the diluted ferrofluids was demonstrated to results from non-interacting single-domain Co particles. In both investigated soft magnetic alloys a concentration profile was found to extend up to $R \approx 1.25\,R'$ around the nanocrystals, which results from enrichment of Nb at the surface of the particles. The magnetization decreases to very low values within this interface, i.e. the direct ferromagnetic exchange interactions with the amorphous matrix must be strongly reduced leaving only weak magnetostatic couplings.

Acknowledgements

Ferrofluide samples were kindly provided by Dr. G. Gansen, Kardiotechnik GmbH, Berlin. The work is partly supported by the DFG project "Colloidal magnetic liquids", No. WI-1151.

References

[1] R.M. Moon, T. Riste, W.C. Koehler, Phys. Rev. 181 (1969) 920.

[2] R. Pynn, J.B. Hayter, Phys. Rev. Lett. 51 (1983) 710.
[3] A. Wiedenmann, J. Appl. Crystallogr. 33 (2000) 428.
[4] B. Toperverg et al., preprint PNPI-2071, 1995, 1.
[5] J. Kohlbrecher, A. Wiedenmann, H. Wollenberger, Z. Phys. 104 (1997) 1.
[6] Th. Keller, A. Wiedenmann, Th. Krist, F. Mezei, Nucl. Instrum. and Meth. A 451 (2000) 474.
[7] A. Wiedenmann, U. Lembke, A. Hoell, R. Muller, W. Schuppel, Nanostruct. Mater. 601–604 (1999).
[8] J. Kohlbrecher, A. Wiedenmann, H. Wollenberger, Mater. Sci. Forum 225–227 (1996) 677.
[9] A. Heinemann, H. Hermann, A. Wiedenmann, N. Mattern, K. Wetzig, J. Appl. Crystallogr. 33 (2000) 1386.
[10] J. Marcin, A. Wiedenmann, I. Skorvanek, Physica B 276–278 (2000) 870.